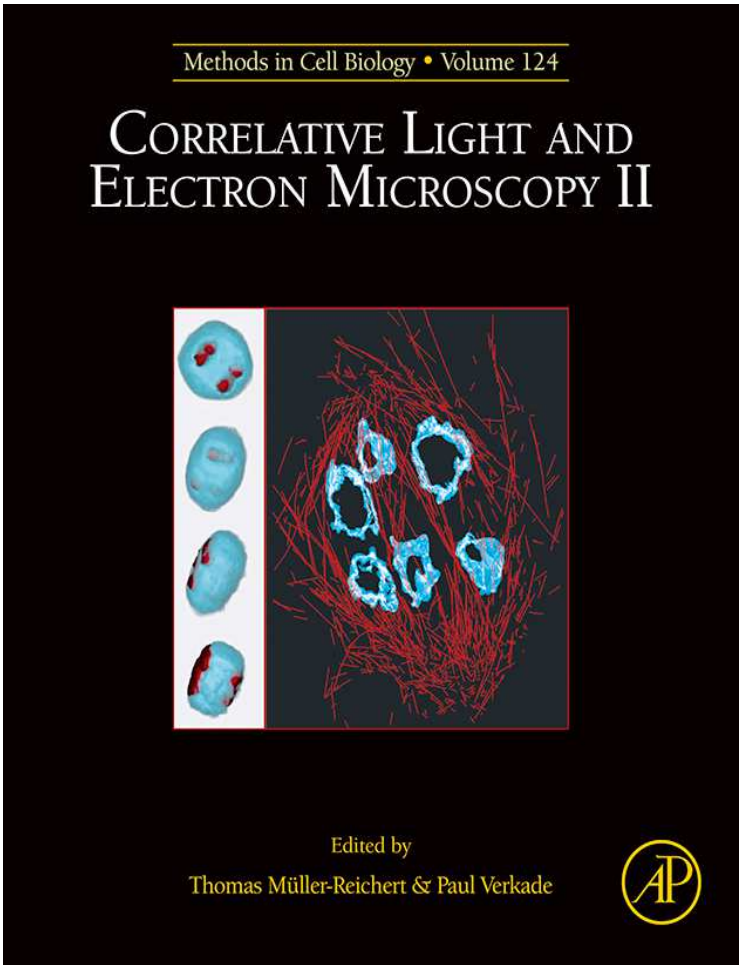

From Kimberley H. Gibson, Daniela Vorkel, Jana Meissner and Jean-Marc Verbavatz, Fluorescing the Electron: Strategies in Correlative Experimental Design. In: Thomas Müller-Reichert and Paul Verkade, editors, *Methods in Cell Biology, Vol. 124*, Burlington: Academic Press, 2014, pp. 23-54.
ISBN: 978-0-12-801075-4

Academic Press

CHAPTER

Fluorescing the Electron: Strategies in Correlative Experimental Design

2

Kimberley H. Gibson, Daniela Vorkel, Jana Meissner, Jean-Marc Verbavatz
Max Planck Institute of Molecular Cell Biology and Genetics, Dresden, Germany

CHAPTER OUTLINE

Methods in Cell Biology, Volume 124, ISSN 0091-679X, http://dx.doi.org/10.1016/B978-0-12-801075-4.00002-1

Abstract

Correlative light and electron microscopy (CLEM) encompasses a growing number of imaging techniques aiming to combine the benefits of light microscopy, which allows routine labeling of molecules and live-cell imaging of fluorescently tagged proteins with the resolution and ultrastructural detail provided by electron microscopy (EM). Here we review three different strategies that are commonly used in CLEM and we illustrate each approach with one detailed example of their application. The focus is on different options for sample preparation with their respective benefits as well as on the imaging workflows that can be used. The three strategies cover: (1) the combination of live-cell imaging with the high resolution of EM (time-resolved CLEM), (2) the need to identify a fluorescent cell of interest for further exploration by EM (cell sorting), and (3) the subcellular correlation of a fluorescent feature in a cell with its associated ultrastructural features (spatial CLEM). Finally, we discuss future directions for CLEM exploring the possibilities for combining super-resolution microscopy with EM.

Abbreviations

CLEM	correlative light and electron microscopy
EM	electron microscopy
fP	fusion protein
FP	fluorescent protein
GFP	green fluorescent protein
LM	light microscopy
PALM	photoactivated localization microscopy
ROI	region of interest
SEM	scanning electron microscopy
STED	stimulated emission depletion microscopy
STORM	stochastic optical reconstruction microscopy
TEM	transmission electron microscopy
TIRF	total internal reflection fluorescence microscopy
YFP	yellow fluorescent protein

INTRODUCTION

Within the field of biology, a myriad of imaging technologies and techniques have arisen in pursuit of illuminating and identifying specific structures and molecules of interest. Research studies depend more and more on light microscopy (LM) to locate fluorescently tagged molecules like proteins, RNA, DNA, and lipids. While useful and applicable to many purposes, these techniques are limited in that they can only reveal a small selection of tagged or targeted molecules within a cell or a tissue without providing insight into the relationship or context that molecule or associated structure may have with its surroundings. Combining electron microscopy (EM) with the attributes of fluorescence microscopy allows us to provide an ultrastructural context in studying relationships between structure, localization, and function for a wide variety of molecules (Müller-Reichert & Verkade, 2012).

Both LM and EM have their advantages and disadvantages. Fluorescence microscopy can be employed to study fluorescently tagged molecules in live or fixed

biological samples. In diffraction-limited LM, however, the resolution for fluorescent markers and endogenously expressed proteins is approximately 200 nm (*x*- and *y*-axes) which is incapable of resolving smaller biological structures like vesicles, microtubules, or organelle subcompartments (Betzig et al., 2006; Huang, Babcock, & Zhuang, 2010; Patterson, Davidson, Manley, & Lippincott-Schwartz, 2010; Robinson, Takizawa, Pombo, & Cook, 2001). In contrast, high resolutions approaching 1 nm can be achieved with EM using conventional staining methods allowing for better identification of structural details. However, transmission electron microscopy (TEM) depends on the passage of highly accelerated electrons through a very thin film of sample necessitating the use of fixatives and resin embedding or freezing to stabilize the sample so that it can be finely sectioned. Imaging of biological samples with an electron beam also requires *en bloc* staining during fixation steps, or poststaining after sectioning. Both depend on the use of high atomic number heavy metals like osmium, lead, and uranium. Specific labeling of molecules (proteins, RNA, DNA, etc.) by EM is challenging and live-cell imaging is nearly impossible.

Correlative light and electron microscopy (CLEM) incorporates a growing number of techniques evolving out of the need to combine the advantages of both LM (usually fluorescence microscopy) and EM. As is true for any research study, techniques and protocols must be adopted and often adapted to answer the question at hand. Various CLEM techniques have been proposed in the literature. Here, we are considering three standard but general CLEM strategies (Fig. 2.1) that, depending on the exact aim, can be employed and modified to fit a specific purpose. Integral to each strategy is the processing step until which fluorescence properties of the fluorescent probe used must be retained. It should be noted that various types of fixation and preparation steps for EM can denature or bleach fluorophores in a sample (Tables 2.1–2.3). Another issue to consider is the ability to spatially relocate the same cell, structure, or region of interest (ROI) in EM after fluorescence imaging at the desired resolution for correlation.

The first strategy that we consider is where dynamic processes are being observed, or where specific time points in development must be recorded. Cells and tissues have to be in a living state during fluorescence imaging (Polishchuk et al., 2000; Müller-Reichert, Srayko, Hyman, O'Toole, & McDonald, 2007; Woog, White, Büchner, Srayko, & Müller-Reichert, 2010; Fig. 2.1A). For time-resolved correlation, the sample must then be rapidly fixed or cryo-immobilized (i.e., through high-pressure freezing or freeze-plunging) at that critical time point of interest before processing for EM (Guizetti et al., 2011; Pelletier, O'Toole, Schwager, Hyman, & Müller-Reichert, 2006; van Rijnsoever et al., 2008). Chemically fixed cells may be embedded in resin (Polishchuk et al., 2000) or they can be further processed for Tokuyasu cryo-sectioning after fixation if desired (Cortese, Diaspro, & Tacchetti, 2009; Tokuyasu, 1973; Robinson et al., 2001; van Rijnsoever et al., 2008). High-pressure frozen samples can be freeze-substituted with lower concentrations of fluorescence-affecting chemicals like osmium, potassium ferrocyanide, or uranyl acetate (Table 2.1) before resin embedding, if fluorescence needs to be preserved further (Kukulski et al., 2011; Petrovska et al., 2014; Watanabe & Jorgensen, 2012; Watanabe et al., 2011).

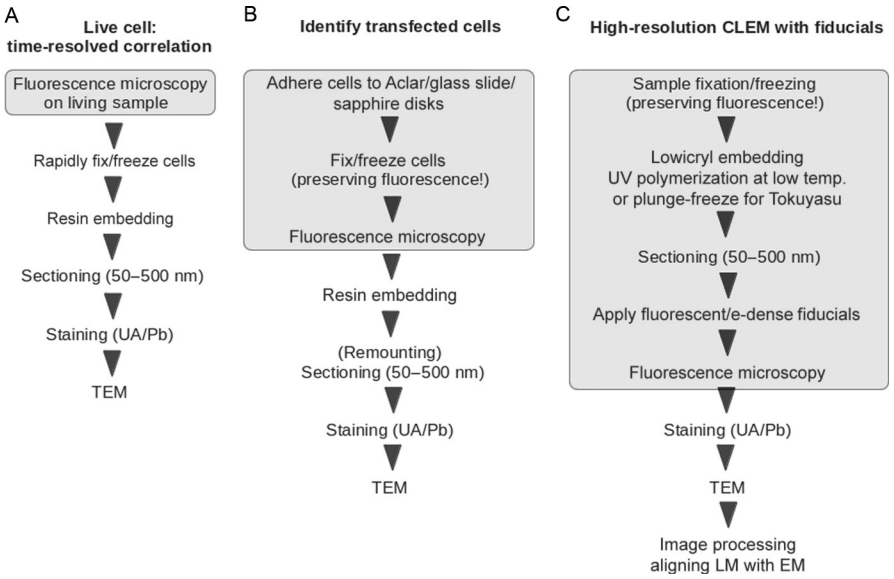

FIGURE 2.1

Three general strategies when considering CLEM in experimental design, where dynamic or development-specific processes must be observed via fluorescence microscopy prior to sample immobilization. (A) LM imaging is performed on living samples after which TEM processing can proceed in samples where transfection rates tend to be lower. (B) Specific fluorescent cells or regions can be detected postfixation via LM before final resin embedding, sectioning, and TEM imaging occur where it is necessary to localize specific subregions within a cell. (C) High-resolution CLEM can be adopted as means of accurately aligning LM with TEM images using fiducials in correlating fluorescently tagged substrates with structures observed in EM. Boxes denote the processing steps where sample fluorescence must be preserved for light microscopy imaging.

A second example of a CLEM strategy is applicable for cell cultures with low transfection rates of a fluorescently tagged protein, where only a fraction of cells may express the protein of interest. Cells exhibiting a phenotype or feature of interest can be identified pre- or postfixation by fluorescence microscopy. Such problematic samples can be adapted for CLEM by adhering cells or tissues to a substrate, such as ACLAR® plastic sheets or glass slides (Guizetti, Mäntler, Müller-Reichert, & Gerlich, 2010; Liv et al., 2013; Polishchuk et al., 2000, van Rijnsoever et al., 2008) for fluorophore-retaining chemical fixation, or on sapphire disks for high-pressure freezing followed directly by fluorescence imaging (Fig. 2.1B). After the fluorescence-identification of transformed cells, the samples can be resin-embedded, then polymerized followed by separation from the adhering substrate, remounted, and then sectioned for TEM imaging.

Table 2.1 List of Chemicals, Their Properties, and Fluorescence-Affecting Concentrations Employed During Chemical Fixation or Freeze-Substitution in CLEM

Chemical or fixative	Fluorescent protein (FP)	Publication	Notable features
Paraformaldehyde (PFA) Aldehyde, cross-linking Negligible autofluorescence	GFP, mCherry, RFP, mEos2, Dronpa, Kaede	Betzig et al. (2006), Hodgson, Tavaré, and Verkade (2014), van Rijnsoever, Oorschot, and Klumperman (2008), Brown, Fetter, Tkachuk, and Clayton (2010), this study	1–5% PFA retains fluorescence in Tokuyasu cryo-sectioning or for low-temperature acrylic resin embedding
Glutaraldehyde (GA) Aldehyde, cross-linking Retains FP fluorescence, but causes autofluorescence Excellent structural preservation	mEos2, Dronpa	Kopek, Shtengel, Xu, Clayton, and Hess (2012), Brown et al. (2010), Watanabe et al. (2011)	0.1–2% GA for excellent structural preservation, but causes autofluorescence that can be quenched using sodium borohydride without quenching FP fluorescence
Osmium tetroxide Very oxidative Membrane contrasting, structural preservation Quenches fluorescence	tdEos, Citrine, GFP, Dendra	Watanabe et al. (2011)	0.001% OsO_4 (with 0.1% $KMnO_4$) in freeze-substitution retains fluorescence, preserving membrane structure; >0.1% OsO_4 in freeze-substitution destroys fluorescence
Potassium permanganate Oxidizer Membrane contrasting, structural preservation	tdEos, Citrine, GFP, Dendra	Watanabe et al. (2011)	0.1% $KMnO_4$ in freeze-substitution retains fluorescence and preserves structure; use of 0.001% OsO_4 with 0.1% $KMnO_4$ preserved both fluorescence and structure
Uranyl acetate (UA) Heavy metal stain	mEos2, Dronpa, GFP, mCherry	Brown et al. (2010), Kukulski et al. (2011), Yuan, Li, Hong, and Hong (2014), Petrovska et al. (2014)	0.1–0.5% UA in freeze-substitution retains FP fluorescence

Continued

Table 2.1 List of Chemicals, Their Properties, and Fluorescence-Affecting Concentrations Employed During Chemical Fixation or Freeze-Substitution in CLEM—cont'd

Chemical or fixative	Fluorescent protein (FP)	Publication	Notable features
Acetone Solvent Mild fixative Scavenges free radicals	GFP, tdEos, Citrine, Dendra, mCherry	Watanabe et al. (2011), this study	100% Acetone quenches fluorescence; recommend adding water (i.e., 5% H_2O) during infiltration, or freeze-substitution. Acetone impedes resin polymerization, so optimally transition into ethanol before resin infiltration
Water Polar solvent Hydration necessary to prevent quenching of fluorescent proteins	GFP, Citrine, Dendra, tdEos	Watanabe et al. (2011)	Inclusion of ~3–5% H_2O during freeze-substitution, infiltration, and acrylic resin embedding helps to retain fluorescence

A third example is applied to the correlation of a fluorescent signal with notable ultrastructural features at the EM level. This issue has often been addressed by employing immunogold labeling in EM in combination with (immuno)fluorescence (Agronskaia et al., 2008; Buser & McDonald, 2010; Cortese, Diaspro, & Tacchetti, 2009; Karreman et al., 2012; Polishchuk et al., 2000; Pranke et al., 2011; Robinson et al., 2001). However, this is not an option for proteins or antigens of interest if no suitable antibody exists. Sometimes, even when antibodies are available, the antigen is not sufficiently abundant at the surface of EM sections to enable detection. The use of semi-thick sections (~150–400 nm) in electron tomography or thicker sections (500–700 nm) in scanning electron microscopy (SEM; Kopek et al., 2012) defeats the point of on-section immunolabeling, which depends on binding of antibodies to antigens exposed only on the surface of a section. However, combining the advantages of fluorescence microscopy with that of EM while superseding the caveats of either technique opens new avenues into illuminating cell ultrastructure and answering many biological queries. To that aim, fluorescently tagged proteins or other fluorescent molecules, like endocytic cargo, can be imaged by fluorescence microscopy, and the fluorescence localization can then be used to reidentify those same subcellular areas of interest with higher-resolution EM (Fig. 2.1C). Such high-resolution CLEM enables us to precisely locate structures or areas within a cell or tissue where

a molecule of interest is targeted. Structural data from EM can then be compared with fluorescence localization information by overlaying the LM and EM images. This strategy requires that we preserve sample fluorescence until after sectioning, when fluorescence imaging can be performed. Sustaining fluorescence in standard EM protocols is tricky as chemical fixation (Table 2.1), freeze-substitution (Tables 2.1 and 2.2), *en bloc* staining (Tables 2.1 and 2.2), and resin embedding (Table 2.3) steps must be designed to minimize cross-linking, oxidation, and photobleaching of the fluorophore without compromising structural preservation. Importantly, certain fluorophores will be more robust after successive chemical treatments than others. An excellent option for fluorescence preservation is to prepare cells or tissues for Tokuyasu or cryo-sectioning technique (Tokuyasu, 1973), which does not require resin embedding.

Given the body of literature on CLEM, we are fortunate that a number of fluorescent proteins, such as green fluorescent protein (GFP), mCherry, mCitrine, Eos, and others, have proven amenably resilient to a wide array of standard and modified

Table 2.2 Cryo-immobilization techniques effectively used in CLEM

Fixation or cryo-immobilization technique	Fluorescent protein (FP)	Publication	Notable features and reagents
Cryo-EM: plunge-freezing (PF)	GFP	Schorb and Briggs (2013)	Cryo-fluorescence imaging on p22 bacteriophages post-FP, followed by cryo-EM
	GFP, mRFP	Duke et al. (2013)	Cryo-fluorescence imaging followed by cryo-soft X-ray tomography
High-pressure freezing (HPF)	EGFP	Watanabe et al. (2011)	GFP fluorescence after HPF followed by direct thawing showed no change in fluorescence level in *C. elegans* Pmyo-2::GFP
HPF, then freeze-substitution	tdEos, Citrine	Watanabe et al. (2011)	0.001% OsO_4 with 0.1% $KMnO_4$ in 95% acetone, ~5% H_2O
	EGFP, mCherry	Kukulski et al. (2011), Yuan et al. (2014), Petrovska et al. (2014)	0.1% Uranyl acetate, in acetone
Chemical fixation (excluding Tokuyasu cryo-prepared samples)	EGFP, mCherry, RFP	This study	3% PFA; 0.2% GA in 1 × PBS buffer; no osmium or uranyl acetate postfixation. Samples embedded in HM20

Table 2.3 List of embedding resins or mediums and their effects on structure and fluorescence

Embedding medium	Fluorescent protein (FP)	Publication	Notable features/ issues
Lowicryl HM20 Nonpolar acrylic resin Low-temperature infiltration Low-temperature UV polymerization Hydrophobic	EGFP; mCherry	Kukulski et al. (2011), Yuan et al. (2014)	Fluorescence is stable after UV polymerization
	Dendra2	Petrovska et al. (2014), this study	Fluorescence bleached due to photoactivation during UV polymerization
Lowicryl K4M Polar, acrylic resin Low-temperature infiltration Low-temperature UV polymerization Hydrophilic	tdEos; mCitrine	Watanabe et al. (2011)	Hydrophilic resin; the use of ~5% H_2O in resin to maintain fluorophore hydration interfered with polymerization, affecting sectioning quality
LR White Acrylic resin High-temperature or low-temperature polymerization UV polymerization optional Hydrophilic	Dendra; tdEos; mEosFP	Watanabe et al. (2011)	Fluorescence quenched due to acidity at pH 5.5; fluorescence retained by stabilizing pH of LR White with ethanolamine; *C. elegans* expressing H2B-tdEos or Dendra used in PALM and then SEM
	mEos2; Dronpa	Kopek et al. (2012), Brown et al. (2010)	Fluorescence retained, but poor mitochondrial structure
LR Gold Acrylic resin Low-temperature polymerization UV polymerization optional Hydrophilic	tdEos; mCitrine	Watanabe et al. (2011)	Poor tissue penetration resulting in poor sectioning
	GFP-immunolabeling only	Buser and McDonald (2010)	Good structural preservation; GFP fluorescence postembedding was not determined
Glycol methacrylate Acrylic (GMA) resin Low-temperature polymerization Hydrophilic	tdEos, mCitrine; Dendra	Watanabe et al. (2011), Watanabe and Jorgensen (2012)	3% H_2O in resin; 70% fluorescence retained; fusion proteins with mCitrine used STED microscopy; tdEos and Dendra were used in PALM, then SEM; inconsistent sectioning due to poor cross-linking

Table 2.3 List of embedding resins or mediums and their effects on structure and fluorescence—cont'd

Embedding medium	Fluorescent protein (FP)	Publication	Notable features/ issues
			of resin with sample exterior
Methylcellulose (Tokuyasu/cryo-sectioning) Chemical fixation Gelatin embedding Sucrose infiltration Plunge-freezing Cryo-sectioning Sections stabilized with methylcellulose	dEosFP, Kaede	Betzig et al. (2006)	0.1% GA/4% PFA fixation, cryo-sectioned, PALM imaging, then embedded in methylcellulose for TEM
	EGFP	Hodgson, Tavaré, and Verkade (2014)	2% PFA/0.2% GA fixation, cryo-sectioning, compare immunolabeling with CLEM
	mGFP; labeled with dextran–Alexa568; or transferrin–Alexa588	van Rijnsoever et al. (2008)	Live-cell fluorescence imaging, cells fixed with 4% PFA/0.05% GA *in situ*, cryo-sectioned, imaged via TEM
	mEos	Kopek et al. (2012)	2% GA; autofluorescence quenched postcryo-sectioning with sodium borohydride
	mEos2; Dronpa	Brown et al. (2010)	No EM, 0.1% glutaraldehyde/4% paraformaldehyde; cryo-embedding/sectioning, then sodium borohydride quenching before fluorescence imaging

EM sample processing techniques, as outlined in Tables 2.1–2.3. From this basis, it is possible to develop multiple strategies to investigate biological questions using a correlative approach.

Once fluorescence-friendly EM protocols have been established, the utility of the method is dependent on our ability to correlate fluorescence signals with precise EM structures for high-resolution CLEM. Tissues and cells are often densely packed with a cornucopia of organelles, undulating membranes, cisternae, fibrillar structures, proteinaceous complexes or arrangements, or budding and blebbing vesicular bodies. If the goal is to isolate fluorescence to any one of these substructures, it must be done with conviction. Not only do we need to relocate the same fluorescence region

in EM that we identified via LM, we also need to accurately align and superimpose the fluorescence signals on the EM structural data to make a comparison. Optimizing the alignment of LM and TEM images requires that we utilize fiducial markers. For CLEM, minute spheres, between 100 and 200 nm in diameter (smaller than LM resolution limit), that are both fluorescent and electron dense for identification in both LM and TEM are excellent fiducials (Kukulski et al., 2011; Petrovska et al., 2014; Schellenberger et al., 2013; Schorb & Briggs, 2013). These can then be used in conjunction with imaging software as reference points to aid in aligning, warping, and overlaying LM and TEM images such that we can make accurate comparisons between the fluorescence localization in LM with the detailed structural data provided via TEM. With these tools in mind, we can consider the variable strategies through which we may further illuminate structures in molecular and cellular context.

2.1 STRATEGIES FOR CLEM

2.1.1 LIVE-CELL IMAGING AND TIME-RESOLVED CORRELATION BETWEEN LIGHT AND ELECTRON MICROSCOPY

Biological processes encompass dynamic events involving localization and translocation of organelles or protein complexes, molecular diffusion and suborganelle sequestration, fusion or fission of membranes, and of course, structural assembly or disassembly. Live-cell imaging allows us to follow specific processes that can occur within short time frames. Those cells or tissues identified at a specific desired stage of the process can be cryo-immobilized or chemically fixed to ensure that the stage in which it is transitioning is preserved. For example, to study Golgi subcompartmentalization and transport, Polishchuk et al. (2000) utilized COS-7 cells transfected with vesicular stomatitis virus G protein (VSVG) that was tagged with GFP. Using confocal microscopy, they observed the procession of the VSVG–GFP from the endoplasmic reticulum (ER) to *trans*-Golgi and post-Golgi after various chemical treatments or temperature shifts. When VSVG–GFP fluorescence dynamics were subcompartmentalized into Golgi-to-plasma membrane (PM) vesicles budding from the Golgi, the cells were then fixed with 4% paraformaldehyde and 0.05% glutaraldehyde while adhered to coverslips. Further confocal imaging followed cell fixation to image fluorescent structures within the *z*-axis. Cells on the coverslips were embedded in resin and later relocated and remounted for serial sectioning, followed by TEM imaging. Stacking the imaged serial sections in *z* followed by segmentation of resulting ER-to-Golgi, *trans*-Golgi, Golgi-to-PM, and also PM-fusion structures provided structural context at various crucial stages in cell trafficking.

Separately, Müller-Reichert et al. (2007) and Woog et al. (2010) embarked on a mission to characterize microtubules in early *Caenorhabditis elegans* embryos undergoing mitosis or meiosis. Live *C. elegans* embryos expressing β-tubulin-GFP, to label the microtubules, and H2B-mCherry, to visualize the chromatin, were observed via fluorescence microscopy (Woog et al., 2010). Embryos entering the

desired stage were then rapidly high-pressure frozen (McDonald, Morphew, Verkade, & Müller-Reichert, 2007) as a means of cryo-preserving them while minimizing ice crystal formation. After freeze-substitution and embedding in resin, they were ensured that each embryo was worth serial sectioning and preparing for investigation via electron tomography. We have used this approach to study the organization of centrosomal microtubules in *C. elegans* embros during metaphase of mitosis. Figure 2.2A shows a fluorescence picture acquired immediately prior to high-pressure freezing. Dual-axis tilt series of serial sections through the centrosomal region (Fig. 2.2B, yellow box) were acquired, reconstructed, and combined (Fig. 2.2C) to allow for further segmentation (Fig. 2.2C and D) and analysis (Fig. 2.2E) of centriolar microtubules (Weber et al., 2012). Using this technique, we can determine with absolute certainty that every embryo sectioned is at the exact time point in the cell cycle, to follow through with further time-consuming EM tomography image acquisition, processing, and analyses.

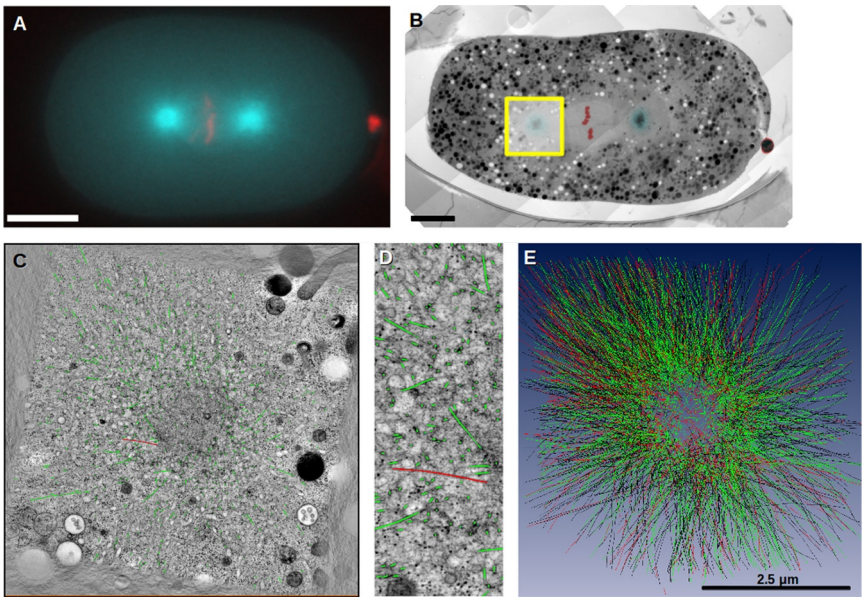

FIGURE 2.2

Imaging of a live *C. elegans* embryo during metaphase just prior to high-pressure freezing. (A) Mitotic spindles in blue, microtubules (MT) labeled by β-tubulin-GFP, and chromatin-labeled H2B-mCherry, red; (B) EM with centrosomes (blue) and chromatin (red) pseudo-colored; yellow box denotes centrosomal area selected for EM tomography; (C) combined dual-axis tomogram showing centrosome with segmented MTs (green lines), red line highlights one MT; (D) enlarged area showing selected MT from C (in red). (E) Three-dimensional model of segmentated microtubules generated by using the ZIBAmira software package.

Similar approaches were utilized by van Rijnsoever et al. (2008) to localize the lysosomal membrane protein LAMP-1-mGFP as expressed in human hepatoma HepG2 cells that were grown on Formvar-coated glass coverslips. The cells were chemically fixed on a coverslip during fluorescence imaging when cells reached the desired stage. Directly after chemical fixation, they proceeded to acquire ~200-nm step confocal image stacks through the *z*-axis of the cell to ease relocation of precise substructures for later TEM imaging. The cells on the coverslip were then processed using a modified Tokuyasu cryo-embedding protocol, followed by cryo-sectioning. The resulting 70-nm-thick serial sections were imaged via TEM and compared with confocal images to ensure subregions were relocated within the fluorescence *z*-stack of the same cell. Testing the utility of live-cell, EM correlated imaging, van Rijnsoever et al. (2008) were able to track and distinguish two differently labeled endosomes in live imaging; one endosome contained either dextran or transferrin-Alexa-568, while another carried both mGFP and either a dextran- or transferrin-bound Alexa568. After observing the motion dynamics of both endosomes, the cell was processed for cryo-immunogold labeling for GFP, which was then relocated via TEM. Here, van Rijnsoever et al. (2008) were able to show the possibility of isolating individual dynamic structures via fluorescence that could later be reidentified in EM for structural analysis.

2.1.2 THE NEEDLE IN A HAYSTACK—IDENTIFICATION OF TRANSFECTED CELLS

Fluorescence microscopy is often used to isolate cells of interest in cell cultures with low frequency, as is often the case for transfected primary culture cells where only a small proportion of cells may be transformed. Cells expressing those genes of interest may show anywhere from marginal to drastic molecular or structural differences, making identification of those details by electron microscopy akin to seeking out a needle in a haystack. Having a means of locating a specific cell transformed with a fluorescent transgene by fluorescence microscopy followed by structural examination with TEM can absolve the aforementioned problems.

We utilized this CLEM strategy in ascertaining the involvement of the vesicle-trafficking protein, Sec22 in ER–PM contact sites in HeLa cells (Petkovic et al., 2014) and neurons.

Neuron cells are not always efficiently transfected. To ensure that we could later relocate an identified fluorescent for TEM investigation, we grew transfected neuron cells on a thin, adherent grated ACLAR® sheet until ~70% confluence was reached (Fig. 2.3). Cells were fixed in place on the ACLAR® sheet with a low concentration of glutaraldehyde to retain fluorescence and preserve ultrastructure (Fig. 2.3A).

Before proceeding through further fixation and embedding steps, cells were prepared by adding a drop of buffer with a coverslip over top of the ACLAR® sheet. Any EGFP-Sec22-expressing cells were located in position on the ACLAR® sheet via epifluorescence microscopy (Fig. 2.3B). The location of the cells on the ACLAR® sheet was noted by imaging landmarks at lower (Fig. 2.3A) and higher magnification

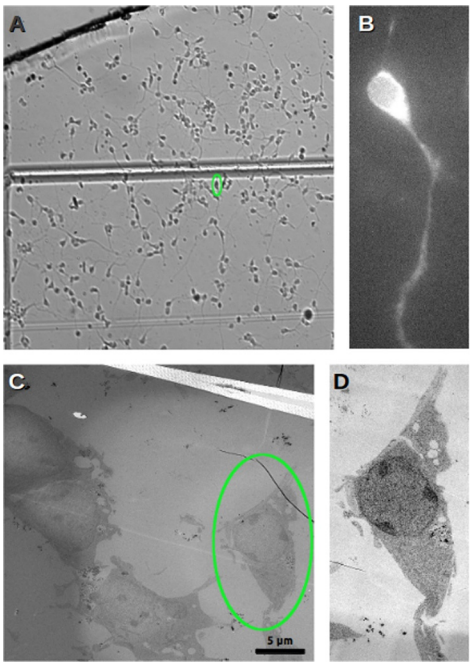

FIGURE 2.3

Locating a transfected neuron expressing GFP-Sec22 via fluorescence for TEM imaging. (A) A 10× bright field image showing aldehyde-fixed neural cells at ~70 confluence on an ACLAR sheet, green ellipse (light gray in the print version) denotes a single fluorescent cell near a grid line etched into the ACLAR sheet; (B) green fluorescence from the same GFP-expressing cell at 100× magnification; followed by (C) relocation of that cell at lower magnification TEM using linear etches as landmarks; before (D) closer examination via TEM of the same cell at higher magnification.

LM using DIC. After LM imaging, the entire ACLAR® sheet was retrieved for further fixation with 1% osmium and flat-embedded in epoxy resin. Throughout all steps described thus far, cells remained adhered in place on the ACLAR® sheet, allowing for ease of relocation after polymerization. The area of resin with identified fluorescent cells was excised from the ACLAR®, remounted on a block, sectioned, and mounted on grids for TEM imaging, ensuring that the cell imaged by TEM was indeed the same cell located in fluorescence microscopy. Here, we were able to relocate the same transfected neuron cell first via fluorescence microscopy for later TEM imaging (Fig. 2.3C), ensuring that the cell was indeed transfected, thereby promoting further examination of this cell (Fig. 2.3D) to ascertain whether any specific transgene-related structural changes could be noted. Following cell relocation, it was demonstrated by electron tomography that Sec22 mediates the apposition of ER and PMs at contact sites (Petkovic et al., 2014).

2.1.3 HIGH-RESOLUTION CLEM FOR PRECISE ALIGNMENT OF FLUORESCENCE AND EM DATA

In subcellular CLEM, the aim is to correlate the fluorescence signal to cell organelle ultrastructure. The optimal methods of preserving fluorescence and ultrastructure involve cryo-techniques. Several different cryo-immobilization methods have been successfully employed in CLEM, including high-pressure freezing, freeze-plunging, and Tokuyasu technique for cryo-sectioning (Table 2.2). High-pressure freezing is an excellent method to preserve fluorescence as it rapidly stabilizes fluorescent proteins without denaturing or photobleaching them (Watanabe et al., 2011). If the sample or tissue is too large to be frozen or not amenable to freezing, then chemical preservation is also an option. The use of chemicals, however, should be carefully considered to minimize damage to the fluorophore (see Table 2.1).

While high-pressure freezing itself does not result in loss of fluorescence (Schorb & Briggs, 2013; Watanabe et al., 2011), the subsequent freeze-substitution and resin-embedding steps can reduce fluorescence through photobleaching, pH changes, dehydration, oxidation, and chemical cross-linking (Katayama, Yamamoto, Mizushima, Yoshimori, & Miyawaki, 2008: Watanabe et al., 2011). The use of osmium tetroxide and glutaraldehyde should be minimized during freeze-substitution so that the ultrastructure is preserved without losing the fluorescent signal or creating too much background autofluorescence. Proteins that we have tested with success include GFP, RFP, and mCherry. Watanabe et al. (2011) preserved the fluorescence of mCitrine or tdEos fused to the histone, H2B and the mitochondrial outer membrane protein, TOM-20 (Watanabe & Jorgensen, 2012) after high-pressure freezing followed by freeze-substitution in 0.001% OsO_4, 0.1% $KMnO_4$ in 95% acetone containing ~5% H_2O. Osmium tetroxide and $KMnO_4$ do cross-link membranes; however, the lower concentrations of each reagent in this cocktail preserved both membrane structure and fluorescence sufficiently enough to enable fluorescence imaging.

It is not recommended to use Lowicryl/Unicryl or even low-temperature formulations of LR White (Brown et al., 2010) if a sample expresses endogenous UV-sensitive monomeric photoswitchable or photoactivatable fluorescence probes (i.e., Dendra2, Kaede, mEos, etc.) as these will likely be photoactivated and then photobleached during the extended 2–3 days of UV resin polymerization. We noted that a protein tagged with Dendra2 failed to retain any fluorescence after HM20 polymerization and sectioning, whereas the same protein tagged with mCherry was easily identified by epifluorescence microscopy. We presently have not tested this protocol on PA-GFP, EosFP, or other photoactivatable or -switchable fluorophores and cannot definitely state whether their fluorophores would survive UV polymerization. Table 2.3 documents effective methods of preserving photoactivatable fluorescent proteins for CLEM, providing alternatives for HM20 (Watanabe et al., 2011). Multimeric photoactivatable fluorophores may prove to be more resistant to photobleaching during UV polymerization as they are not as easily degraded as the more sensitive monomeric forms of some photoactivatable/switchable fluorophores like

Dendra2 or Kaede (Campbell & Davidson, 2010; Patterson et al., 2010; Watanabe et al., 2011). For samples expressing UV-sensitive fluorescent probes of interest, other acrylic resins should be considered. However, the alternative of 60 °C polymerization used for resins including LR Gold and LR White may also destroy some fluorescence.

Watanabe et al. (2011) tested several acrylic resins for their ability to oxidize, photobleach, or preserve fluorescent probes and found that glycol methacrylate (GMA), when mixed with an additional 3% H_2O, preserves fluorescence best in comparison to Lowicryl K4M, LR Gold, and LR White. They noted that adding water to the final GMA resin mixture renews fluorescence by up to 30% of that observed in nonhydrated resin mixtures, highlighting that dehydrated fluorophores are in an inactive nonfluorescent state. Hydration of fluorescent proteins plays an important role in maintaining fluorescence, as does pH. Many fluorescent proteins such as EGFP, Sapphire, and the dsRed derivative, mRFP (S146G) are acid-sensitive, quenching fluorescence between pH 4.3 and 6.2 (Katayama et al., 2008). GMA remains alkaline at pH 8 during polymerization. Another advantage of GMA is that it polymerizes at lower temperatures, between −4 °C and −20 °C without UV light. If samples possessing UV-sensitive fluorescent proteins (i.e., Dendra2, Kaede) are to be processed for fluorescence post-EM embedding, then it would be wise to consider infiltrating with GMA rather than Lowicryl HM20 or K4M.

If worries persist regarding sensitive fluorophores, other methods such as Tokuyasu cryo-ultramicrotomy (see above), with the possibility of including a lower 0.1–0.3% addition of glutaraldehyde, can be considered. If higher concentrations of glutaraldehyde are needed for optimal structural preservation, it is possible to quench autofluorescence postfixation and embedding by incubating sections with sodium borohydride prior to fluorescence acquisition (Brown et al., 2010; Kopek et al., 2012). Fluorescence maintenance in cryo-sections for a wide variety of fluorophores has been extensively documented and is adaptable for CLEM using epifluorescence, confocal, and super-resolution fluorescence microscopy (SRFM) techniques (Betzig et al., 2006; Hodgson, Tavaré, & Verkade, 2014; Kopek et al., 2012; van Rijnsoever et al., 2008). For example, Hodgson, Tavaré, & Verkade, 2014 effectively preserved and localized the EGFP-tagged GLUT4 to the PM in adipose cells prepared using the Tokuyasu method. Betzig et al. (2006), Brown et al. (2010), and Kopek et al. (2012) showed that cryo-sections are able to withstand the extensive imaging times used for SRFM techniques such as photoactivated localization microscopy (PALM).

To obtain fluorescence information useful for comparison with EM ultrastructure, we want to strategically align the fluorescently tagged protein or molecule within a more precise structural context observed in EM. The sample processing strategy must simultaneously prolong fluorescence and minimize sample shifting between fluorescence and EM imaging steps. We are no longer simply interested in whether a cell or tissue is expressing a protein of interest indicative of its transformed status. We now have to preserve fluorescence in our sample as we process it using standard EM methodologies, while also ensuring that we can relocate fluorescence-associated structures within ultrastructure-dense electron micrographs. To that aim,

fiducial markers have been used. Fiducials are spherical points that can be applied to the sections on a grid that are then used to identify those regions on the grid at higher magnifications. CLEM alignment requires that the fiducials are both fluorescent and electron dense, so that we can see the same fiducials in LM and then later at higher TEM magnifications. For example, Blue FluoSphere® (Molecular Probes, Inc., Leiden, The Netherlands) fiducials were used by Kukulski et al. (2011). These can be used with green or red cellular fluorescent markers. Schellenberger et al. (2013) and Schorb and Briggs (2013) opted to use multichannel fluorescent 100-nm TetraSpeck™ microspheres (Life Technologies, Carlsbad, CA, USA) as fiducial markers allowing for fluorescence emission in red, green, and blue channels. These 100-nm beads are also sufficiently electron dense enough to be visualized by TEM. Both Schellenberger et al. (2013) and Schorb and Briggs (2013) tested fluorescent fiducial alignment procedures using fluorescently tagged viral particles that were plunge-frozen for cryo-fluorescence microscopy followed by cryo-electron tomography. Schellenberger et al. (2013) tested chromatic shifts or mechanical stage shifts in *x*- and *y*-axes when using multi-color (red–green–blue) emitting TetraSpeck™ beads. They found, on average, ~150-nm shift between the same beads imaged in green and blue channels. For the same beads imaged in red and blue channels, they noticed even higher average ~300–400-nm shift. For high-precision CLEM image alignment, especially when imaging closely associated structures in multichannel fluorescence imaging, it is recommended to first align images acquired in different channels to one another before proceeding to align fluorescence image data with that of EM images. Given the nature of Formvar and plastic thin sections, there is much room for stretching, shrinking, and warping of plastic surfaces between grid bars, between cells, and between LM and EM imaging. Using an alignment program that can account for elastic warping in distances between fiducial markers selected in LM images versus EM images is essential.

We are now challenged with translating suboptimal fluorescence resolution (~200 nm) onto an electron micrograph with resolutions varying between 1 and 20 nm (Kukulski et al., 2011; Schellenberger et al., 2013; Schorb & Briggs, 2013). This can be problematic if fluorescently tagged proteins localize to areas of a cell where many organelles are densely packed, interlinked, or compartmentalized, confusing attempts to correlate fluorescence localization with a specific organelle or region of the cell.

For suspension cultures, we have applied high-pressure freezing. We tested a modified freeze-substitution protocol adapted from Kukulski et al. (2011) to prepare yeast cells that had been transfected with an EGFP-tagged amphipathic lipid-sensing domain of synapsin previously described by Krabben et al. (2011) and explored further by Pranke et al. (2011). This domain interacts with highly curved membranes, such as those comprising vesicular surfaces, playing a role in binding and aggregating synaptic vesicles in neurons. Transformed yeast cells were freeze-substituted and embedded in HM20 resin. We found fluorescence difficult to detect in thin sections (i.e., <120 nm thick) and sections thicker than 150 nm will be difficult to resolve by TEM unless electron tomography is used. Therefore, we used 150-nm-thick sections, labeled with 200-nm diameter Blue FluoSpheres used as fiducial markers for

correlation between LM and EM. Given that many of our proteins of interest were endogenously tagged with GFP or mCherry (Petrovska et al., 2014), having fluorescent fiducials that, when quenched, were mostly fluorescing in only the UV-blue channel was optimal. Second, the 200 nm polystyrene-based Blue FluoSpheres® were of sufficient electron density to be easily observed via electron microscopy rendering them useful in aligning areas of interest in TEM with LM images. We acquired images at either 10× or using a 100× (1.4 NA) oil immersion lens with an upright epifluorescence microscope at excitation/emission of 500/520 for blue, for the fiducials, and 488/514 for GFP (Fig. 2.4A). Images were also acquired in bright field DIC and overlaid on the low-magnification TEM image (Fig. 2.4C),

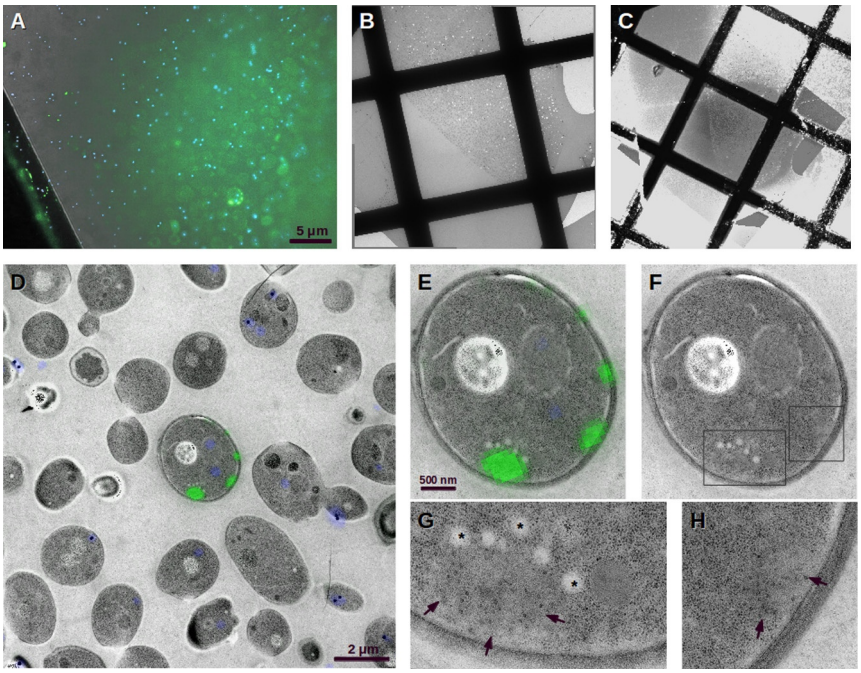

FIGURE 2.4

Investigation of structures associated with a synapsin-EGFP fusion protein in yeast. (A) 100× LM images of synapsin-GFP, green fluorescence, overlayed with 200 nm Blue FluoSphere fiducials, blue fluorescence, on a DIC image; (B) 100× TEM micrograph, 2 × 2 montage of the same ROI as identified by LM; (C) 100× TEM image overlayed on 10× DIC image; (D) GFP signal and blue fiducials correlated to a subregion in 11,000× TEM micrograph; (E) TEM image of yeast cell with correlated GFP signal; (F) TEM image without fluorescent channels, GFP-correlated regions in boxes; (G) bottom-center subregion from (F) showing vesicle clusters in a ribosome-exclusion zone adjacent to the plasma membrane; (H) bottom-right subregion from (F) highlighting similar structure as seen in (G). Vesicle clusters: arrows; cortical ER: asterisks.

to visualize grid bars and landmarks on the Formvar surface. We relocated the same area where the fluorescent cell was located in TEM, first by finding and imaging the same ROI at lower 100× TEM magnification (Fig. 2.4B). To distinguish between densely packed yeast cells, we performed a rough alignment using the lower magnification 10× DIC image with the 100× TEM image (Fig. 2.4C). After noting the subregion within the TEM image where our fluorescent cell was located, we acquired montages at higher magnifications (~1–2 nm pixel size) in TEM (Fig. 2.4D and E). Using the blue-electron-dense fiducials, we aligned the LM and TEM images such that we were able to identify the precise location of the synapsin-GFP chimera in the yeast cell (Fig. 2.4E). The GFP signal correlated exactly with clusters of vesicles within the yeast cell (Fig. 2.4F) that were always found laying adjacent the PM (Fig. 2.4G and H). For the alignment of fiducials, we used the Amira imaging software package (FEI Company, the Netherlands; Fig. 2.5).

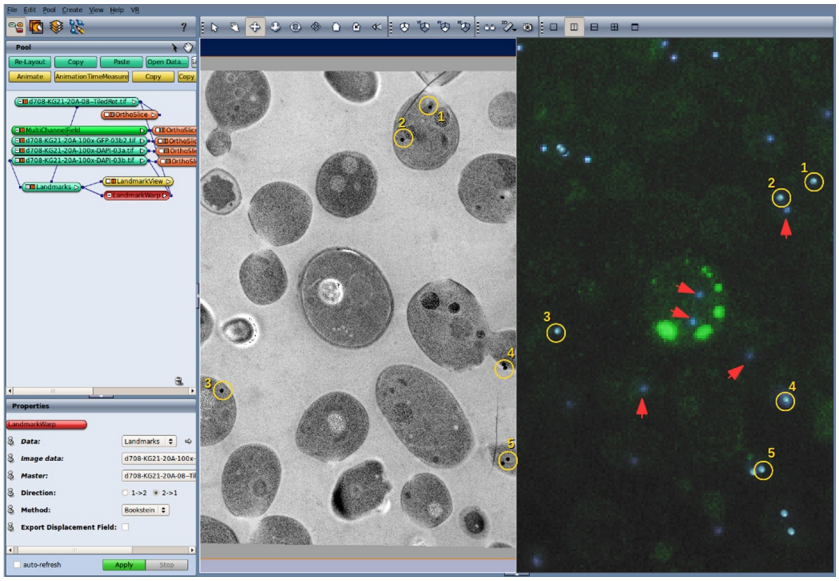

FIGURE 2.5

Screen capture of the Amira imaging software interface with imported TEM image (center panel) and fluorescence (right panel) images. Using the MultiChannelField, the epifluorescence alpha-channel images of GFP (green) and Blue FluoSpheres (DAPI channel, blue) are pseudo-colored. Using the LandMark (2 sets) module in Amira, electron-dense spheres corresponding to FluoSphere fiducials are selected as landmark points consecutively in first, the EM image, and then the fluorescence image (yellow circles surrounding pale blue selected "landmark" points). When a sufficient number of points have been selected, the fluorescence image is LandMarkWarped (registered) to the EM image. Red arrows denote FluoSpheres that detached between fluorescence and TEM imaging.

While this provides exceptionally powerful data regarding fluorescent protein localization, there were a few problems arising with the alignment procedure. Between fluorescence and TEM imaging, there were several steps through which the grid was treated with water or other reagents, in rinsing away the glass slide mounting medium or during staining with lead citrate. During these steps, some of the FluoSpheres dislodged from the Formvar-section surface and were either rinsed away (blue fluorescent "shadows" in Figs. 2.4D and E and 2.5, right panel) or relocated elsewhere on the grid. Most of the fiducials remained in place, still allowing for accurate alignment between LM and EM.

2.1.4 STAINING FOR TEM

Once samples have been imaged for fluorescence, then poststaining with either or both lead citrate and uranyl acetate can be performed. Karreman et al. (2012) tested the resilience of the fluorescent dye, TRITC after poststaining with 0.2% uranyl acetate and found a 68% reduction in fluorescence intensity while fluorescence lifetime was lowered by 25%. Consider that, due to interactions between the heavy metal stains and the fluorophore, the option to acquire any further fluorescence data after poststaining the grid is not worthwhile. Standard staining procedures employed for uranyl acetate and lead citrate are applicable at this stage of CLEM procedure.

2.2 METHODS

2.2.1 CRYO-IMMOBILIZATION AND SEGMENTATION OF MICROTUBULES IN MITOTIC SPINDLES IN *C. elegans* EMBRYOS BY ELECTRON TOMOGRAPHY

The protocols for fluorescence imaging, high-pressure freezing and freeze-substitution followed by electron tomography, and tilt-series acquisition were documented in detail by Müller-Reichert et al. (2007) and Woog et al. (2010). Computational tools for microtubule segmentation and analysis are described further by Torsney-Weir et al. (2011), Weber et al. (2012), and Redemann et al. (2014).

2.2.2 LOCALIZATION OF EGFP-SEC22-TRANSFECTED NEURON CELLS

1. Etch a grid-like design onto an ACLAR sheet using a razor blade or fine-gauged syringe needle. This grid will be used as a reference guide to aid in later relocation of transfected cells.
2. Coat the etched-surface of the ACLAR sheet with 0.1% poly-L-lysine to aid in culture cell adherence. Allow solution to dry.
3. Place the ACLAR sheet, etch-side facing up, onto the bottom of a culture dish. We use 6-well plates.
4. Cortical neuron cells were dissected and dissociated before being plated in MEM loading medium on ACLAR sheets within a 6-well cell culture plate.

After 2 h of attachment to the ACLAR sheets, the culture medium is changed to neurobasal medium (with B27 and glutamine). Cells are then transfected at DIVI with GFP or GFP-Sec22b (Petkovic et al., 2014) and allowed to incubate for 24 h allowing for expression.

5. While adhered to the ACLAR sheets, cells are fixed with 0.1% glutaraldehyde and 1% paraformaldehyde in 1 × PBS buffer for 30 min to 1 h. The sheets are rinsed three times with 1 × PBS buffer.
6. A droplet of 1 × PBS is applied to the ACLAR sheet with preserved cells, and a coverslip is laid on top of the ACLAR for fluorescence imaging.
7. Cells expressing EGFP-tagged Sec22p are identified and located via fluorescence microscopy followed by bright field microscopy so as to allow for later relocation of nonfluorescent cells, structural details, and razor-blade etches on the ACLAR sheet.
8. Cells are imaged by LM at low (4 × or 10 ×) and higher (63 × dry, or 100 ×, 1.4 NA, oil immersion) magnification.
9. After LM imaging, the coverslip is gently pried from the ACLAR surface. A few droplets of filtered water are added at the edge of the ACLAR sheet and coverslip. The tip of a forceps is wedged between the two surfaces to help break surface tension so as to not dislodge cells. The ACLAR sheet is washed with ddH_2O for approximately 20 min.
10. Cells on the ACLAR sheet are incubated with 1% OsO_4 reduced with 0.15% potassium ferrocyanide for 60–120 min at room temperature.
11. The ACLAR sheet is washed three times with ddH_2O.
12. Dehydration series are performed: 50% ethanol, 70%, 80%, 90%, 96% followed by three changes in 100% anhydrous ethanol with 10 min per step at room temperature.
13. The ACLAR sheet is transitioned from 100% ethanol into increasing concentrations of Epon Lx112 or your epoxy resin of choice. Three transition steps comprised of 1:3 (v/v), followed by 1:1 (v/v), and then 2:3 (v/v) of ethanol-to-Lx112 resin are performed for 1 h per incubation.
14. Cells are infiltrated for ~4 h or overnight with 100% Epon Lx112.
15. The ACLAR sheet is then embedded in 100% Epon Lx112 and laid in a thin layer of resin followed by polymerization at 60 °C for ~48 h.
16. Due to the strong adherence of the neuron cells to the ACLAR sheet, cells have remained in their original positions throughout the fluorescence imaging and subsequent fixation, dehydration, and resin-embedding steps. Surface details, grid patterns, and lines drawn on the ACLAR sheet can be identified using a dissection microscope to relocate general areas where fluorescent cells of interest were identified prior to osmium fixation.
17. Areas where cells of interest were located are sliced out of the ACLAR sheet using a razor blade. Areas with cells of interest are remounted on an epoxy-based dummy block using a two-phase Epoxy 907 Adhesive System to stably hold the sample in place.

18. Section the area with cell(s) of interest. Here, we use a Leica UCT Ultramicrotome and transfer 70-nm-thick (thin sections) or 300-nm-thick (tomography) sections onto Formvar-coated copper slot grids.
19. Grids are stained with uranyl acetate and lead citrate and then imaged with a Tecnai-12 BioTwin TEM (FEI Company, Eindhoven, the Netherlands) for thin sections or a Tecnai F30 TEM (FEI Company) for electron tomography:
    - Cells originally identified by fluorescence microscopy are located at lower/medium TEM magnifications (between 300× through 3000×) by comparing the arrangement of cells adjacent, ACLAR sheet grid marks or etches, and other notable features.
    - The cell(s) of interest are imaged at higher TEM magnifications.

2.2.3 HIGH-RESOLUTION CLEM: SAMPLE PREPARATION, SECTIONING, IMAGE ACQUISITION, AND ALIGNMENT

1. *Saccharomyces cerevisiae* cells transformed with a synapsin-GFP fusion protein (fP) are inoculated into an $S_{Glucose-Ura+Doxycycline}$ (as a repressor) culture and grown overnight at 30 °C. Cells are backdiluted into fresh $S_{Glucose-Ura}$ medium containing no Doxycycline and grown until log phase ($OD_{600} = 0.3–0.5$).
2. Concentrate the cell culture by gentle vacuum filtration with 0.45-m HV Durapore® Membrane Filters (Merck Millipore, Millerica, MA, USA) in a Vacuum Filtering Flask (Merck Millipore) with a 125-mL capacity Glass Microanalysis Filter Holder (Merck Millipore).
3. After filtration, concentrated cells are kept moist on the filter paper by readdition of 30–50 μL unfiltered growth medium every 15 min to prevent cell dehydration before high-pressure freezing.
4. For high-pressure freezing, we use 0.1 × 1.5-mm membrane carriers (Leica Microsystems) in concert with the Leica EM PACT2 high-pressure freezing machine with a rapid transfer system (Leica Microsystems). Before freezing, 0.5 μL of 20% bovine serum albumin (BSA) dissolved in H_2O is transferred to the membrane carrier to act as a cryo-protectant.
5. Scrape a small blob of filtered yeast from the filter paper using a toothpick. Mix the yeast cells with the 20% BSA solution in the membrane carrier. Immediately transfer the membrane carrier into the EM PACT2 for high-pressure freezing.
6. After freezing, membrane carriers are maintained under liquid N_2 to prevent ice crystal formation until freeze-substitution can be performed.
7. Freeze-substitution is carried out using a Leica AFS2 (Leica Microsystems) machine. Membrane carriers are transferred into a freeze-substitution cocktail containing 0.1% uranyl acetate, 2–4% H_2O, in distilled acetone. The premade cocktail is stored in 1 mL aliquots in cryo-vials under liquid N_2 until needed.

8. Sample processing initiates with a −90 °C step lasting 50–58 h before transitioning to −45 °C over 9 h. Within the 2 h −45 °C step, the cocktail is rinsed twice with prechilled 100% acetone (distilled) before transitioning into prechilled 100% anhydrous ethanol. For yeast or other cells cultured in 0.5–2% glucose-based mediums, it is best to use ethanol to dissolve remaining cytosolic glucose, which impedes acrylic and/or epoxy resin infiltration (Buser & McDonald, 2010).
9. Within the AFS2 machine, sample membrane carriers are transferred from the cryo-vials and positioned within a Leica Flow-through ring in a Reagent bath (Leica Microsystems) container to ease reagent handling and subsequent polymerization of samples. Insert the membrane carriers with the sample facing upward. Prechilled anhydrous ethanol is added to the Flow-through ring to ensure that sample carriers remain moist during transfer.
10. For fluorescence preservation, freeze-substituted samples are embedded in low-temperature Lowicryl HM-20 acrylic resin. This resin can be infiltrated into samples between −45 °C and −25 °C, followed by UV polymerization at −25 °C for 48–56 h. Due to the toxicity and volatility of HM-20, it is recommended to install the AFS2 machine in a walk-in fumehood, or adapt a mobile fumehood with air filtration system over top of the AFS2 sample chamber. Beginning at −45 °C, sample carriers are infiltrated with 10% HM-20 in anhydrous ethanol followed by 25% HM-20, then 50%, 75% and then 100% HM-20 over a 10–12 h period until reaching −-25 °C. Three changes with 100% HM-20 are made over a ∼24 h period.
11. To facilitate HM-20 polymerization under hypoxic conditions, an ACLAR foil (Leica Microsystems) is laid over top of the Flow-through ring (Leica Microsystems) after filling the Flow-through ring and Reagent bath with fresh HM-20. The samples are polymerized in the AFS2 machine with the UV LED lamphousing (Leica Microsystems) at −25 ºC for 48–56 h.
12. After polymerization, sample cylinder blocks with membrane carriers still attached are sliced from the plastic Flow-through ring using a razor blade.
13. Membrane carriers are separated from the sample cylinder blocks by shearing HM-20 resin from the base of the membrane carrier and then gently prying the carrier from the base of the cylinder, leaving the yeast sample embedded in the cylinder. The entire cylinder with the embedded yeast cells can now be mounted into an ultramicrotome chuck for sectioning.

2.2.3.1 Sectioning and fiducial application

1. Sections are cut with an Ultracut UCT Microtome (Leica) set to the ∼150 nm thickness range and then mounted on Formvar-coated 100-mesh copper grids. To facilitate section relocation in LM and TEM, try to place sections in the center of the grid. Ensure that grids have some feature allowing for relocation of grid spaces in LM and EM. For example, often square Cu grids have an “arrow” in the center. Do not use slot grids, as Formvar films tend to break when retrieving the

grid from the glass slide mounting medium after fluorescence microscopy imaging. Slot grids also lack useful features necessary for relocation and orientation of ROIs for CLEM.

2. Apply fluorescent fiduciary markers to the section surface. We use Invitrogen Molecular Probes™ Blue FluoSphere® fiducials, 200 nm diameter. It is recommended to quench the Blue FluoSpheres® as the spheres are highly fluorescent in the Blue/UV/Cyan/Green epifluorescence channels and can often obfuscate identification of any fluorescently tagged protein. This can be done with 0.1% Tween 20 for 10 min, followed by two washes in PBS (Kukulski et al., 2011). To prevent clustering, sonicate the solution immediately prior to use.

2.2.3.2 Fluorescence microscopy

1. Mount the grid, section side up, on a glass slide in 30 μL of nonhardening mounting medium with coverslip (we use Vectashield® Vector Laboratories, Peterborough, UK).
2. Find the center of grid at low magnification (i.e., 10×) in bright field, noting orientation of grid on a sheet of paper. Drawing a diagram or printing a large picture of your grid from the manufacturer's Web site upon which you can sketch locations will help relocate ROIs later in TEM.
3. Proceed to higher magnification lens (i.e., 100×, 1.4 NA, oil immersion) using only transmitted light to avoid photobleaching the sample, recheck the grid diagram for orientation (i.e., find central "arrow"). Avoid selecting and imaging areas near the edge of the grid. These peripheral areas will be more difficult to reacquire later in TEM due to mechanical limitations in *x*/*y*-axis TEM stage motion.
4. Isolate fluorescently tagged structures on sections in fluorescent channel(s) specific to fluorescent marker (i.e., GFP, dsRed, mCherry, etc.).
5. Once an ROI has been located, acquire an image in the appropriate channel(s). Without moving the stage, image the same ROI under a Blue filter to acquire fiducial fluorescence. Given that regions between grid bars where Formvar/ sections are unsupported and are therefore, not flat, often only part of the ROI will be in focus. Try to acquire several images in the same ROI in the same epifluorescence channel using different focusing steps to ensure that as many areas within the ROI are in focus. Ensure that you have acquired all relevant fluorescent channels before moving the stage to seek out a new ROI.
6. When removing the grid from the glass slide/coverslip, use a syringe filled with ddH_2O and 0.2-μm filter with needle attached to apply water near the edge of the coverslip and slide. It is important to avoid damaging the Formvar film and sections on the grid.
7. Wedge the tip of forceps between the slip and the slide to gently and slowly pry the coverslip away from the slide. The water should seep in between the slip and slide to break the cohesion-tension of the Vectashield® mounting medium.
8. Pick the grid up with forceps, clamping the grid in place by applying tension in the forceps with a rubber O-ring. Holding the grid vertically over a surface,

rinse the grid with filtered ddH_2O by allowing single droplets to fall onto the grid from the filter–syringe–needle. Draw excess water off with a wedge of filter paper and allow the grid to air dry.

9. Post-stain with lead citrate for 3 min.

2.2.3.3 TEM imaging

For CLEM, a setup that can acquire montaged images encompassing a larger field of view is optimal to simplify correlation of EM with LM images. First, we perform an initial LM-to-EM alignment using a large field of view TEM image in order to ascertain which cells are actually worth imaging at higher magnification. This can be done at low magnification.

1. Take EM micrographs at lower magnification to acquire an ROI (montaging if necessary) approximating the fluorescence microscopy field of view at 100× magnification. The magnification should be high enough to identify the fiducials: use a pixel size of ~10 nm. The ROI should show notable features, such as cell orientation, shape, size, with respect to section edges or to grid bars.
2. Do a rough alignment of the montaged image with the fluorescence images (Blue FluoSphere fiducials and GFP/mCherry, etc.), using appropriate software Fiji/ImageJ or Amira. The rough CLEM overlayed image is used to identify any specific subregions within the TEM image that are worth acquiring at higher TEM magnifications.
3. When interesting subregions within the ROI are identified using the aligned LM and low-magnification TEM image, return to the TEM to acquire higher magnification images at the final resolution. Montaging can again be used to cover the desired field of view. One possibility is to directly transfer the LM image data (Fluorescence and DIC/Widefield, etc.) to the TEM computer: open the LM data in SerialEM (http://bio3d.colorado.edu/SerialEM/) and use the Registration Points option to align selected areas in the LM images to low/medium-magnification TEM images acquired with SerialEM (Schorb & Briggs, 2013).
4. Once interesting subregions have been located in roughly correlated low-magnification LM/TEM images, high-magnification TEM images can immediately be acquired.

2.2.3.4 High-resolution CLEM image alignment

For LM/TEM alignment purposes, several programs can be used to align or overlay fluorescence and TEM images using fiducials. Section warping due to stretching and shrinking of plastic embedding resin incurred during sectioning, grid handling, staining, and electron beam damage will affect the alignment procedure. It is important to choose a program that can account for minute elastic shifts in subregions of an ROI between LM and TEM imaging. To this end, we have employed the LandMarkWarp module or subprogram within the Amira (FEI Company, Eindhoven, the Netherlands) imaging software (Fig. 2.5).

1. Open both fluorescence LM and EM images in Amira and display them side by side in two display windows.
2. Using the LandMarkWarp function, select fiducials pairs (one in LM and one in EM) that correspond to those same fluorescent sphere.
3. Warp and overlay the LM image onto the TEM image with confidence that our fluorescence data actually correspond to specific structures observed in TEM. Other options include using the Landmark and Registration (elastic stack alignment) plugins in Fiji/ImageJ (http://fiji.sc/Fiji).

2.3 MATERIALS

2.3.1 REAGENTS

Chemicals from EMS, Science Services GmbH, München, Germany: 100% acetone, distilled; 16% paraformaldehyde (aqueous EM grade); 25% glutaraldehyde (EM grade, distillation, purified); Formvar (15/95 Resin powder); lead citrate and Epon LX112 Epoxy resin kit; Cryo-Lok, cryogenic vials (2.0 mL); Lowicryl HM-20 kit, ACLAR® fluoropolymer film, copper slot grids (2 mm × 1 mm slot), 100-mesh square copper grids, and uranyl acetate (Polysciences, Inc., Eppelheim, Germany). Potassium hexacyanoferrate (III) trihydrate (Sigma-Aldrich Chemie GmbH, Munich, Germany). 6-Well cell culture plate (Merck Millipore, Millerica, MA, USA). Two-Part Epoxy Adhesive Kit, Epoxy 907 Adhesive System (Miller-Stephenson Chemical Company, Inc., Sylmar, CA, USA). Bovine serum albumin, Fraction V (Sigma-Aldrich Chemie GmbH, Munich, Germany). The fluorescent fiducials described were 0.2-μm diameter Blue (365/415) FluoSphere® Fluorescent Microspheres (Molecular Probes, Inc., Leiden, The Netherlands). For LM, grids were mounted in Vectashield® H-1000 mounting medium (Vector Laboratories, Inc., Burlingame, CA, USA).

2.3.2 CELL CULTURES

S. cerevisiae BY4742 transformed with a construct encoding the amphipathic synaptic vesicle targeting region of synapsin (amino acids 69–96) (Krabben et al., 2011) fused to a portion of the coiled coil region of GMAP210 (amino acids 39–375), followed by yEGFP. Cells were cultured in S-medium minus Ura, with 2% Glucose. Mouse cortical neuron primary cells were initially grown in loading medium (MEM, fetal calf serum, glutamine, and glucose) and then in neurobasal medium supplemented with B27 and glutamine. Culturing conditions and GFP-Sec22-related constructs are described in more detail by Petkovic et al. (2014).

2.3.3 LIGHT MICROSCOPY

LM images were acquired with an upright Zeiss Axioplan2 epifluorescence microscope (Carl Zeiss, Oberkochen, Germany), with Metaview imaging software (Visitron Systems, Puchheim, Germany).

2.3.4 ELECTRON MICROSCOPY AND IMAGE PROCESSING

High-pressure freezing, and freeze-substitution supplies were from Leica Microsystems GmbH, Wetzlar, Germany: EMPACT2 high-pressure freezing machine, membrane carrier 1.5 mm × 0.1 mm, AFS2 freeze-substitution machine, UV lamphousing with LEDs, Reagent bath, Flow-through rings, and ACLAR® foils. Sectioning was performed using an Ultracut UCT Microtome (Leica). We employed a Tecnai-12 BioTwin TEM operated at 100 kV (FEI Company, Eindhoven, NL), with an axial Tietz F214A CCD camera (TVIPS GmbH, Gauting, Germany). With this camera, we have the option of using either EM-Menu 4.0 (TVIPS) software or SerialEM (http://bio3d.colorado.edu/SerialEM/index.html) to acquire TEM images. Either software can produce montaged or tiled images. Dual-axis electron tomography tilt series were acquired on a 300 kV Tecnai G2 F30 Twin TEM (FEI Company) with a bottom-mounted Gatan US 1000 CCD camera (Roper Scientific) with SerialEM (http://bio3d.colorado.edu/SerialEM/). Tilt series were reconstructed and the two axes were combined in IMOD (http://bio3d.colorado.edu/imod/). Centrosomal microtubules were segmented using the automated MicrotubuleTracing module and Segmentation Editor (Redemann et al., 2014; Torsney-Weir et al., 2011; Weber et al., 2012) within the ZIBAmira imaging software package (Zuse Institute Berlin, Germany). The automated MicrotubuleTracing software is also available online: http://amitube.mpi-cbg.de/. Image processing for the alignment of fiducials between LM and EM was also done in ZIBAmira.

2.4 DISCUSSION

Here we have reviewed and described three general directions. In the first approach, we have combined live-cell imaging and electron microscopy to study the 3D organization of microtubules during cell division. The purpose is to use EM resolution to trace individual microtubules in a densely crowded environment at a very precise time point in the cell cycle. This approach requires rapid fixing of the sample at the time point of interest. To that aim, we have used high-pressure freezing, but chemical fixation is also possible. The advantage of this time-resolved approach is that we know the exact state of the cell before processing it for EM. However, there is no direct spatial correlation between LM and EM images of the sample. In the second example, we used fluorescence microscopy to initially locate a cell of interest among hundreds for further examination at the EM level. This form of "cell sorting" allows us to address the issue of phenotypic variability in transfected cell cultures to definitively identify transfected cells from untransfected cells. Further EM processing and subsequent EM-level imaging can then be performed on the fluorescence-identified cells of interest. The third approach described herein involves spatial correlation of LM and EM data and is more challenging as it requires higher precision correlation.

Instead of separating the LM and TEM imaging steps, one could employ the new Tecnai™ iCorr TEM (FEI Company, Eindhoven, the Netherlands) which is

adapted from a standard FEI Tecnai TEM platform, where an additional 15× objective lens with fluorescence excitation ranging from 460 to 500 nm has been integrated into the TEM column, allowing for rapid and consecutive acquisition of fluorescence and TEM image data on the same EM grid, within the same apparatus. Interestingly, the iCorr™ system can be adapted for use in cryo-electron microscopy allowing for investigation of fluorescence-tagged proteins retained after freeze-plunging followed by acquisition within the same TEM. The cryo-adaptability of the iCorr™ system is especially useful given that antibodies cannot be applied to frozen sections, preventing the use of immunolabeling. For cryo-EM, only endogenously labeled samples can be used. For resin-embedded samples, Agronskaia et al. (2008) used a precursor to the iCorr system, the integrated Laser and Electron Microscope, to localize Alexa488-labeled catalase in peroxisomes of rat liver cells. To further the use of this technology, Karreman et al. (2012) considered the effects of low-vacuum conditions on various dyes, noting that certain dyes were optimally fluorescent when hydrated. They tested the fluorescence intensity of Alexa488, Alexa532, Cy2, Cy3, FITC, and TRITC in water or N_2 gas (to mimic low-vacuum, TEM conditions), finding that Cy2 and TRITC were the most stable, along with Cy3 and FITC, in N_2.

We have described our protocol with the intent of examining our samples via TEM. However, there is no reason that the protocols described herein could not be similarly examined using SEM. Serial sections of the same cell identified by LM could then be reexamined by SEM. Liv et al. (2013) integrated a 100×, 1.4 NA objective lens inside the vacuum chamber of a SEM, below the sample in an inverted epifluorescence LM configuration. A 470 nm LED provided illumination for fluorophore excitation. To study cell-to-cell interactions, they labeled actin in adenocarcinoma cells with phalloidin–Alexa488 or cortactin–Alexa488 and were able to identify higher concentrations of the fluorescent markers in extrusions or fine lamellar outgrowths. Provided poststaining of the sample does not interfere with the fluorescence signal, this approach could be used for either low- or high-resolution correlation between LM and EM, possible as an alternative to using fiducials.

Finally, it should be noted that all the methods described above are compatible with 3D imaging in EM, using for instance electron tomography (Guizetti et al., 2011; Pelletier et al., 2006; Petkovic et al., 2014; Swulius & Jensen, 2012) or SEM (Kopek et al., 2012).

Some limitations of the approaches described here should also be considered. For instance, fluorescent protein fusions have previously been noted to contribute to mislocalization, misfolding, and dimerization, resulting in structural artifacts when tagged to proteins of interest (Coumans et al., 2013; Katayama et al., 2008; Quattrocchino, Spelt, & Koes, 2013). Some fluorescent proteins, notably multimeric DsRed and GFP and other *Aequorea victoria*-derived fluorescent variants, can dimerize at higher concentrations in a cell (Von Stette, Noireclerc-Savoye, Goedhard, Gadella, & Royant, 2012) which can interfere with localization or substrate binding, thereby raising issues with regard to fluorescence imaging and quantification. Von Stette et al. (2012) developed an obligately monomeric version of

cyan fluorescent protein, called mTurquise presenting an A206K mutation; other researchers have used this same mutation to render yellow fluorescent protein (YFP) into mCitrine, GFP into m(E)GFP and mVenus, and the red mCherry. Many transgenic systems involve overexpression of said fluorescent fPs also resulting in structural or biochemical changes not at all representative of the biological system under study (Comley et al., 2011; Coumans et al., 2013). Untargeted DsRed and its derivatives, mRFP and zFP506, were found to accumulate in lysosomes while retaining fluorescence (Katayama et al., 2008). Merely expressing untagged GFP in breast cancer cells induced a myriad of proteomic changes resulting in altered expression of proteins involved in protein folding, immune response, and cytoskeleton regulation (Coumans et al., 2013). YFP expression was also implicated in increasing gene expression for proteins involved in oxidative/metabolic stress, inflammation, and apoptosis signaling neurons of transgenic mice (Comley et al., 2011). Swulius and Jensen (2012) reported that the helical cytoskeleton described in previous studies utilizing YFP tagged to the actin-homolog MreB in *Escherichia coli* MC1000/pLE7 is an artifact of the YFP tag. Using cryo-electron tomography, they examined and compared untransformed wild-type *E. coli* pLE7 with cells expressing native MreB, to MreB-YFP, and MreB tagged with mCherry and found that only YFP-tagged cells exhibited filamentous structures adjacent the inner membrane of the cells. In lieu of this finding, they suggested that much of the literature surrounding helical cytoskeleton studies with YFP-MreB fPs in bacteria ranging from *Bacillus subtilis*, *Caulobacter crescentus*, and *Vibrio cholerae* should be reconsidered.

Similarly, we encountered fluorescent protein-induced structural alterations when studying the aggregative capabilities of the glutamine synthesis, mCherry fP (Petrovska et al., 2014). In considering potential structural artifacts, we compared fP-mCherry-transformed yeast cells with those expressing the photoactivatable Dendra2-fP or those with untagged fP. We found striking differences in the cytosolic filaments found in the mCherry fusion versus the Dendra2-fused and nonfused Gln1. In spite of these structural differences, our CLEM strategy could not be pursued using Dendra2-tagged protein because it did not survive the final extended 48 h of UV-light exposure required to polymerize the Lowicryl HM20 resin in which the yeast cells were embedded. In lieu of this, we could have embedded cells in a different resin, such as GMA, described earlier.

These artifacts are difficult to avoid, but they can be detected by testing multiple approaches and comparing the results. By preserving, at minimum, two samples: the first expressing the protein of interest with a fluorescent tag and the second expressing the protein of interest, alone, we can test the degree of structural interference induced by that fluorescent probe using electron microscopy. Given that not all fluorescent tags are alike, comparing fluorescence patterns of different fluorescent protein fusions (i.e., GFP, YFP, mCitrine, mCherry, DsRed, Dendra, mEosFP, etc.) followed by TEM or SEM examination is useful to affirm the degree to which a particular fluorescent probe interferes with the structure and localization of a given protein of interest.

2.4.1 TOWARD SUPER-RESOLUTION CLEM

While high-resolution CLEM overcomes many previous barriers in localizing specific fluorescent signals to specific structures in EM, the best fluorescence resolution that can be obtained with standard epifluorescence, confocal, or spinning disk LM is approximately ~200 nm in the *x*-/*y*-axes and ~400–600 nm in the *z*-axis. When comparing closely associated structures at the EM level using correlative fluorescence signal for that locale, the lower LM resolution limits the degree to which we can definitively state that a fluorescent signal corresponds to a specific structure or subregion within an aligned electron micrograph. Even by fluorescence microscopy standards, the 200 nm limit in the *x*/*y*-resolution impedes that ability to precisely localize or colocalize fluorescently tagged molecules, even when they target to different subcompartments or trafficking pathways. This limitation is well recognized and over the past decade, it has been giving rise to the development of several technologies and techniques. SRFM depends on the ability to separate individual fluorescent probes or molecules not only in space but also over time, so that individual molecules can be imaged. Enabling many SRFM techniques like PALM, STORM, or stimulated emission depletion microscopy (STED) is the employment of photoactivatable, photoswitchable, or photoblinking fluorescent probes that can be repeatedly, through targeted doses of fluorescent light, activated and deactivated before finally photobleaching (Betzig et al., 2006; Herbert, Soares, Zimmer, & Henriques, 2012; Patterson et al., 2010; Watanabe & Jorgensen, 2012). These comprise some of the most demanding imaging techniques involving extended fluorophore excitation and acquisition times. Already, SRFM techniques have been employed in CLEM techniques, rendering the fluorescence resolution comparable to EM resolution in ways that provide more meaningful correlative structural localization data than previously attainable by more established epifluorescence or confocal microscopy methods. Betzig et al. (2006) demonstrated localization of cytochrome *c* oxidase tagged with dEosFP using total internal reflection fluorescence microscopy (TIRF) and PALM on cryo-prepared thin-section COS-7 cells. They relocated and aligned the PALM image with a TEM image, showing sublocalization of cytochrome *c* oxidase in mitochondrial matrices. Watanabe and Jorgensen (2012) localized a tdEos-tagged TOM-20 in *C. elegans* mitochondria using PALM followed by SEM on thin sections. Watanabe et al. (2011) further compared resolution and fluorescence localization in confocal, STED, TIRF, and PALM using the histone, H2B and outer mitochondrial membrane protein, TOM20 fused to either Citrine or tdEos. Fluorescent patterns identified in the highest resolution fluorescence imaging techniques, STED and PALM were relocated and correlated in EM, with a precision exceeding that of standard epifluorescence, confocal, and TIRF microscopy. Furthering the exploration of mitochondrial subcompartmental localization, Kopek et al. (2012) tagged TFAM, a mitochondrial DNA-binding protein, with mEos2 in mouse 3T3sw fibroblast cells. They coupled PALM fluorescence data with correlational focused ion beam SEM 3D imaging on Tokuyasu cryo-sections, isolating TFAM in mitochondrial nucleoids. Expanding on these examples, we can imagine a myriad of applications for super-resolution in future CLEM studies.

ACKNOWLEDGMENTS

The authors wish to thank Dr. Cathy Jackson for permitting the use of yeast cells as well as Simon Alberti, Doris Richter, Ivana Petrovska, Matthias Munder, and Liliana Malinovska for aiding with yeast culturing methods, reagents, and discussions.

REFERENCES

Agronskaia, A. V., Valentijn, J. A., van Driel, L. F., Schneijdenberg, C. T. W. M., Humbel, B. M., van Bergen en Henegouwen, P. M. P., et al. (2008). Integrated fluorescence and transmission electron microscopy. *Journal of Structural Biology*, *164*, 183–189.

Betzig, E., Patterson, G. H., Sougrat, R., Lindwasser, O. W., Olenych, S., Bonifacino, J. S., et al. (2006). Imaging intracellular fluorescent proteins at nanometer resolution. *Science*, *313*, 1642–1645.

Brown, T. A., Fetter, R. D., Tkachuk, A. N., & Clayton, D. A. (2010). Approaches to super-resolution fluorescence imaging of mitochondrial proteins using PALM. *Methods*, *51*, 458–463.

Buser, C., & McDonald, K. (2010). Correlative GFP-immunolocalization microscopy in yeast. *Methods in Enzymology*, *470*, 603–618.

Campbell, R. E., & Davidson, M. W. (2010). Part I. Types of imaging reporter genes. Chapter 1. Fluorescent reporter proteins. In S. S. Gambhir, & S. S. Yaghoubi (Eds.), *Molecular imaging with reporter genes* (pp. 3–40). New York: Cambridge University Press.

Comley, L. H., Wishart, T. M., Baxter, B., Murray, L. M., Nimmo, A., Thomson, D., et al. (2011). Induction of stress in neurons from transgenic mice expressing yellow fluorescent protein: Implications for neurodegeneration research. *PLoS One*, *6*(3), e17639.

Cortese, K., Diaspro, A., & Tacchetti, C. (2009). Advanced correlative light/electron microscopy: Current methods and new developments using Tokuyasu cryosections. *Journal of Histochemistry & Cytochemistry*, *57*(12), 1103–1112.

Coumans, J. V. E., Gau, D., Poljak, A., Wasinger, V., Roy, P., & Moens, P. (2013). Green fluorescent protein expression triggers proteome changes in breast cancer cells. *Experimental Cell Research*, *320*(2014), 33–45.

Duke, E. M. H., Razi, M., Weston, A., Guttman, P., Werner, S., Henzler, K., et al. (2013). Imaging endosomes and autophagosomes in whole mammalian cells using correlative cryo-fluorescence and cryo-soft X-ray microscopy (cryo-CLXM). *Ultramicroscopy*, *143*, 77–87. http://dx.doi.org/10.1016/j.ultramic.2013.10.006.

Guizetti, J., Mäntler, J., Müller-Reichert, T., & Gerlich, D. W. (2010). Correlative time-lapse imaging and electron microscopy to study abscission in HeLa cells. *Methods in Cell Biology*, *96*, 591–601.

Guizetti, J., Schermelleh, L., Mäntler, J., Maar, S., Poser, I., Leonhardt, H., et al. (2011). Cortical constriction during abscission involves helices of ESCRT-III-dependent filaments. *Science*, *331*, 1616–1620.

Herbert, S., Soares, H., Zimmer, C., & Henriques, R. (2012). Single-molecule localization super-resolution microscopy: Deeper and faster. *Microscopy and Microanalysis*, *18*(6), 1419–1429.

Hodgson, L., Tavaré, J., & Verkade, P. (2014). Development of a quantitative correlative light electron microscopy technique to study GLUT4 trafficking. *Protoplasma*, *251*(2), 403–416.

Huang, B., Babcock, H., & Zhuang, X. (2010). Breaking the diffraction barrier: Super-resolution imaging of cells. *Cell*, *143*, 1047–1058.

Karreman, M. A., Agronskaia, A. V., van Donselaar, E. G., Vocking, K., Fereidouni, F., Humbel, B. M., et al. (2012). Optimizing immuno-labelling for correlative fluorescence and electron microscopy on a single specimen. *Journal of Structural Biology*, *180*, 382–386.

Katayama, H., Yamamoto, A., Mizushima, N., Yoshimori, T., & Miyawaki, A. (2008). GFP-like proteins stably accumulate in lysosomes. *Cell Structure and Function*, *33*, 1–12.

Kopek, B. G., Shtengel, G., Xu, C. S., Clayton, D. A., & Hess, H. F. (2012). Correlative 3D superresolution fluorescence and electron microscopy reveal the relationship of mitochondrial nucleoids to membranes. *Proceedings of the National Academy of Sciences of the United States of America*, *109*(16), 6136–6141.

Krabben, L., Fassio, A., Bhatia, V. K., Pechstein, A., Onofri, F., Fadda, M., et al. (2011). Synapsin I senses membrane curvature by an amphipathic lipid packing sensor motif. *Journal of Neuroscience*, *31*, 18149–18154.

Kukulski, W., Schorb, M., Welsch, S., Picco, A., Kaksonen, M., & Briggs, J. A. (2011). Correlated fluorescence and 3D electron microscopy with high sensitivity and spatial precision. *Journal of Cell Biology*, *192*(1), 111–119.

Liv, N., Zonnevylle, A. C., Narvaez, A. C., Effting, A. P. J., Voorneveld, P. W., Lucas, M. S., et al. (2013). Simultaneous correlative scanning electron and high NA fluorescence microscopy. *PLoS One*, *8*(2), e55707.

McDonald, K. L., Morphew, M., Verkade, P., & Müller-Reichert, T. (2007). Recent advances in high-pressure freezing. In J. Kuo (Ed.), *Electron microscopy, methods and protocols: 369*. *Methods in molecular biology* (pp. 143–173) (2nd ed.). Totowa, NJ: Humana Press Inc. (Chapter 8).

Müller-Reichert, T., Srayko, M., Hyman, A., O'Toole, E. T., & McDonald, K. (2007). Correlative light and electron microscopy of early *Caenorhabditis elegans* embryos in mitosis. *Methods in Cell Biology*, *79*, 101–119.

Müller-Reichert, T., & Verkade, P. (Eds.), (2012). Correlative light and electron microscopy. In *Methods in cell biology: Vol. 111*. (pp. 1–460). Elsevier Inc., Oxford, UK: Academic Press.

Patterson, G., Davidson, M., Manley, S., & Lippincott-Schwartz, J. (2010). Superresolution imaging using single-molecule localization. *Annual Review of Physical Chemistry*, *61*, 345–367.

Pelletier, L., O'Toole, E., Schwager, A., Hyman, A. A., & Müller-Reichert, T. (2006). Centriole assembly in *Caenorhabditis elegans*. *Nature*, *444*, 619–623.

Petkovic, M., Jemaiel, A., Daste, F., Specht, C. G., Izeddin, I., Vorkel, D., et al. (2014). The SNARE Sec22b has a non-fusogenic function in plasma membrane expansion. *Nature Cell Biology*, *16*(5), 434–444.

Petrovska, I., Nüske, E., Munder, M. C., Kulasegaran, G., Malinovska, L., Kroschwald, S., et al. (2014). Filament formation by metabolic enzymes is a specific adaptation to an advanced state of cellular starvation. *eLife*, *3*, e02409.

Polishchuk, R. S., Polishchuk, E. V., Marra, P., Alberti, S., Buccione, R., Luini, A., et al. (2000). Correlative light-electron microscopy reveals the tubular-saccular ultrastructure of carriers operating between Golgi apparatus and plasma membrane. *The Journal of Cell Biology*, *148*(1), 45–58.

Pranke, I. M., Morello, V., Bigay, J., Gibson, K., Verbavatz, J. M., Antonny, B., et al. (2011). α-Synuclein and ALPS motifs are membrane curvature sensors whose contrasting chemistry mediates selective vesicle binding. *Journal of Cell Biology*, *194*(1), 89–103.

Quattrocchino, F. M., Spelt, C., & Koes, R. (2013). Transgenes and protein localization: Myths and legends. *Trends in Plant Science*, *18*(9), 473–476.

Redemann, S., Weber, B., Möller, M., Verbavatz, J. M., Hyman, A. A., Baum, D., et al. (2014). The segmentation of microtubules in electron tomograms using amira. *Methods in Molecular Biology*, *1136*, 261–278.

Robinson, J. M., Takizawa, T., Pombo, A., & Cook, P. R. (2001). Correlative fluorescence and electron microscopy on ultrathin cryo-sections: Bridging the resolution gap. *Journal of Histochemistry and Cytochemistry*, *49*, 803–808.

Schellenberger, P., Kaufman, R., Siebert, C. A., Hagen, C., Wodrich, H., & Grünewald, K. (2013). High-precision correlative fluorescence and electron cryo microscopy using two independent alignment markers. *Ultramicroscopy*, *143*, 41–51. http://dx.doi.org/10.1016/j.ultramic.2013.10.011.

Schorb, M., & Briggs, J. A. G. (2013). Correlated cryo-fluorescence and cryo-electron microscope with high spatial precision and improved sensitivity. *Ultramicroscopy*, *143*, 24–32, pii: S0304-3991(13)00291-X.

Swulius, M. T., & Jensen, G. J. (2012). The helical MreB cytoskeleton in Escherichia coli MC1000/pLE7 is an artifact of the N-terminal yellow fluorescent protein tag. *Journal of Bacteriology*, *194*(23), 6382–6386.

Tokuyasu, K. (1973). Technique for ultracryotomy of cell suspensions and tissues. *Journal of Cell Biology*, *57*, 551–565.

Torsney-Weir, T., Saad, A., Möller, T., Weber, B., Hege, H. C., Verbavatz, J. M., et al. (2011). Tuner: Principled parameter finding for image segmentation algorithms using visual response surface exploration. *IEEE Transactions on Visualization and Computer Graphics*, *17*(12), 1892–1901.

van Rijnsoever, C., Oorschot, V., & Klumperman, J. (2008). Correlative light-electron microscopy (CLEM) combining live-cell imaging and immunolabelling of ultrathin cryosections. *Nature Methods*, *5*(11), 973–980.

Von Stette, D., Noireclerc-Savoye, M., Goedhard, J., Gadella, T. W. J., Jr., & Royant, A. (2012). Structure of a fluorescent protein from *Aequorea victoria* bearing the obligate-monomer mutation A206K. *Acta Crystallographica*, *F68*, 878–882.

Watanabe, S., & Jorgensen, E. M. (2012). Visualizing proteins in electron micrographs at nanometer resolution. *Methods in Cell Biology*, *111*, 298–306 (Chapter 15).

Watanabe, S., Punge, A., Hollopeter, G., Willig, K., Hobson, R. J., Davis, M. W., et al. (2011). Protein localization in electron micrographs using fluorescence microscopy. *Nature Methods*, *8*(1), 80–84.

Weber, B., Greenan, G., Prohaska, S., Baum, D., Hege, H. C., Müller-Reichert, T., et al. (2012). Automated tracing of microtubules in electron tomograms of plastic embedded samples in *Caenorhabditis elegans* embryos. *Journal of Structural Biology*, *178*(2), 129–138.

Woog, I., White, S., Büchner, M., Srayko, M., & Müller-Reichert, T. (2010). Correlative light and electron microscopy of intermediate stages of meiotic spindle assembly in the early *Caenorhabditis elegans* embryo. *Methods in Cell Biology*, *111*, 223–234 (Chapter 12).

Yuan, Y., Li, M., Hong, N., & Hong, Y. (2014). Correlative light and electron microscopic analyses of mitochondrial distribution in blastomeres of early fish embryos. *The FASEB Journal*, *28*, 577–585.